Synergistic Effect of Ag and Pd Ions on Shape-Selective Growth of Polyhedral Au Nanocrystals with High-Index Facets

ARTICLE *in* THE JOURNAL OF PHYSICAL CHEMISTRY C · FEBRUARY 2011

Impact Factor: 4.77 · DOI: 10.1021/jp111997s

2 AUTHORS:

Toan Trong Tran
University of Technology Sydney
9 PUBLICATIONS **73** CITATIONS
SEE PROFILE

Xianmao Lu
National University of Singapore
83 PUBLICATIONS **5,432** CITATIONS
SEE PROFILE

THE JOURNAL OF PHYSICAL CHEMISTRY C

ARTICLE

pubs.acs.org/JPCC

Synergistic Effect of Ag and Pd Ions on Shape-Selective Growth of Polyhedral Au Nanocrystals with High-Index Facets

Toan Trong Tran and Xianmao Lu*

Department of Chemical and Biomolecular Engineering, National University of Singapore, Singapore 117576

Supporting Information

ABSTRACT: We report the synergistic effect of two foreign metal ions, Pd(II) and Ag(I), on the shape-selective growth of polyhedral gold nanocrystals in a facile one-pot polyol synthesis. By varying the concentrations of Ag(I) and Pd(II) in a growth solution containing $HAuCl_4$, gold nanocrystals were formed in high yields (>90%) with tailored shapes including truncated tetrahexahedra (THHs) bounded by {310} and {111} facets, truncated ditetragonal prisms (DTPs) enclosed by 12 {310} facets, and multiple-twinned bipyramids. We found that when Ag(I) and Pd(II) are introduced separately, Ag underpotential deposition (UPD) induces the formation of Au {110} facets, while Pd deposition facilitates the development of Au {100} facets. The combination of the two foreign metal ions leads to a completely different nanocrystal growth mode. At low concentrations of Ag(I), the addition of Pd(II) causes the appearance of Au {310} facets. Depending on the ratio of Ag(I)/Pd(II), single-crystalline Au nanocrystals either partially or entirely enclosed by {310} facets are formed. At high concentrations of Ag(I), multiple-twinned bipyramids are obtained. Elemental analyses indicated that these nanocrystals are mainly composed of Au (>96 at. %) with a small amount of Ag and Pd.

INTRODUCTION

Shape-selective synthesis of noble metal nanocrystals has attracted much attention in recent years due to their shape-dependent properties and wide variety of applications.[1−5] Among various approaches to tune the geometry of metal nanocrystals,[6−20] the introduction of foreign metal ions in solution-phase syntheses has shown a drastic morphology-selection effect.[21−27] This strategy has been most successfully demonstrated in the gold−silver system where the presence of Ag(I) in trace amount has induced the formation of Au nanocrystals with various shapes.[28−36] This shape-controlling effect was first discovered by Murphy and co-workers who used Ag(I) in a seed-mediated synthetic approach to improve the yield of Au nanorods.[28] Yang et al. also applied this strategy to a polyol synthesis and successfully obtained Au nanocubes.[37] More recently, the use of Ag(I) has been extended to the preparation of Au octahedra,[30,32] rhombic dodecahedra,[35] bipyramids,[29,31] high-index tetrahexahedra (THH),[34] and concave cubes.[38] The influence of Ag ions on the growth of Au nanocrystals has been attributed to underpotential deposition (UPD) of Ag on Au surfaces causing the appearance of high-energy facets.[22,29] In addition to Ag, other metals ions such as Cu(II) have also shown shape-selective effect in the synthesis of Au nanocrystals.[27]

It is well-known that the deposition mode of one metal on another metal surface can be significantly affected by their physicochemical properties such as atomic radii and bond dissociation energies.[39] Therefore, if two foreign metal species are introduced simultaneously in a Au nanocrystal growth process, their different deposition behaviors may interfere with each other[40] and give rise to unusual shape-selective effect. This would allow great flexibility on controlling the shape of the nanocrystals. However, to date, the use of foreign metal ions in Au nanocrystal synthesis has been mainly investigated for systems involving one foreign metal species. Here, we report the first study of the synergistic effect of two foreign metal ions on tuning the shape of Au nanocrystals. In this work, both silver and palladium ions are used in a one-pot poly(diallyldimethylammonium chloride) (PDDA)-mediated polyol process to grow polyhedral gold particles. The deposition of Pd on Au nanocrystals has been of great interest due to their intriguing catalytic properties, although focus has been mainly on Pd−Au bimetallic alloy or core−shell nanostructures.[39,41−48] When both Ag(I) and Pd(II) ions are present in the Au nanocrystal growth solution, we have observed a shape-selective effect in stark contrast to that of Ag(I) or Pd(II) ions alone. By simply varying the atomic ratio of Ag(I)/Pd(II), a series of Au nanostructures including truncated ditetragonal nanoprisms enclosed by {310} facets, truncated tetrahexahedra (THHs) with both {111} and {310} facets, and bipyramids in high yields have been synthesized. The truncated ditetragonal prism (DTP) with high-index {310} facets is a novel polyhedral shape, which has not been reported for Au nanocrystals before.

MATERIALS AND METHODS

Materials. Ethylene glycol (EG, Sigma-Aldrich), chloroauric acid trihydrate ($HAuCl_4 \cdot 3H_2O$, Alfa Aesa), silver nitrate ($AgNO_3$, Sigma-Aldrich), palladium(II) chloride ($PdCl_2$, Alfa Aesar), poly(diallyldimethylammonium chloride) aqueous solution (PDDA, 20 wt %, MW = 200 000−350 000, Sigma-Aldrich), hydrochloric acid (37%, Merck), and sodium chloride (Sigma-Aldrich) were used as received. Ten millimolar H_2PdCl_4 solution was prepared by dissolving 35.6 mg of $PdCl_2$ in 20 mL of 20 mM

Received: December 17, 2010
Revised: January 19, 2011
Published: February 11, 2011

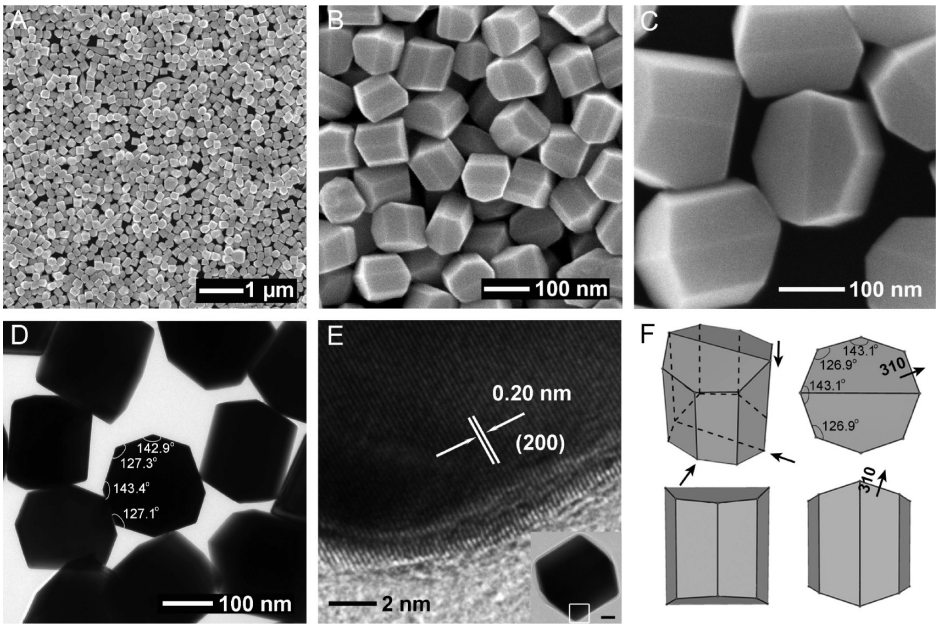

Figure 1. (A) Low- and (B,C) high-magnification SEM images of Au nanocrystals synthesized with a ratio of Au:Pd:Ag = 15:1:1.6 at 120 °C. The nanocrystals exhibit a truncated ditetragonal prism (DTP) shape. (D) TEM image of the Au nanocrystals. The measured angles between the edge-on side faces of one DTP are indicated. (E) HRTEM of a Au nanocrystal exhibiting [100] principal axis. (F) Schematic drawing of a truncated DTP enclosed with {310} facets and its projections along the three indicated viewing angles.

HCl at 100 °C to form a transparent solution. The water used throughout this work was 18.2 mΩ ultrapure deionized water.

Synthesis of Au Nanocrystals. In a typical synthesis of Au truncated ditetragonal prisms, 0.2 mL of PDDA solution and 10 mL of EG were mixed in a glass vial under stirring at room temperature. To this solution were added 18.8 μL of 0.5 M $HAuCl_4$, 2 μL of 500 mM $AgNO_3$, 62.5 μL of 10 mM H_2PdCl_4, and 430 μL of deionized H_2O. The final concentrations of Au, Pd, and Ag were 0.9, 0.06, and 0.096 mM, respectively (molar ratio of Au:Pd:Ag = 15:1:1.6). It was found that adding 10 μL of 1 M NaCl aqueous solutions to the reactions could further improve the yield. The vial was then capped tightly and heated in an oil bath at 120 °C for 12 h with stirring. The solution color changed from yellow to colorless gradually after 2 h. After 3.5 h, the solution became pale pink and finally stopped at reddish brown at 12 h. The product was harvested by centrifugation and washed with acetone once and with water five times to remove excess PDDA. The as-synthesized Au nanocrystals were finally stored in water for further uses.

A similar synthetic procedure was followed for Au bipyramids, except that the Ag(I) concentration was increased to 0.48 mM by adding 10 μL of 500 mM $AgNO_3$ (molar ratio of Au:Pd:Ag = 15:1:8). For the reactions of truncated tetrahexahedra, Ag(I) concentration was reduced to 0.024 mM (molar ratio of Au:Pd:Ag = 15:1:0.4). Note that a purification step was carried out in the case of Au truncated tetrahexahedra to remove a minor amount of large-size Au octahedra, and a washing with saturated NaCl was applied for Au bipyramids to remove residual AgCl.

Characterizations. Scanning electron microscopy (SEM) images were taken using a JEOL JSM-6700F operating at 10 kV. Transmission electron microscopy (TEM) images, selected area electron diffraction (SAED) patterns, and energy dispersive X-ray spectroscopy (EDX) spectra were acquired on a JEOL JEM-2010F operating at 200 kV. High-resolution transmission electron microscopy (HRTEM) images were obtained using a JEOL JEM-2100F operating at 200 kV. Samples for TEM and SEM were prepared by drop casting the sample solutions onto carbon-coated copper grids and silicon substrates, respectively. These samples were then rinsed with a copious amount of deionized water to remove excess polymers and dried at 60 °C. The X-ray diffraction (XRD) spectra were acquired using a Shimadzu XRD-6000 diffractometer equipped with a Cu Kα radiation source (λ = 1.5418 Å) from samples deposited onto a plastic substrate. The scan rate and step size were 1 deg/min and 0.02°, respectively. UV−visible spectra of the Au nanocrystals were recorded using a Shimadzu UV-1601 spectrometer with plastic cuvettes of 1 cm path length at room temperature. X-ray photoelectron spectroscopy (XPS) analyses were performed using a Kratos AXIS Ultra DLD spectrometer equipped with an Al Kα monochromatized X-ray source with a penetration depth of around 3 nm. Inductively coupled plasma mass spectrometry (ICP-MS) measurements were carried out with an Agilent 7500 ICP-MS instrument. Samples were prepared by dissolving the nanocrystals using freshly made aqua regia followed by diluting in DI H_2O.

RESULTS AND DISCUSSION

Figure 1A−D shows representative SEM and TEM images of the Au nanocrystals obtained from reactions with a molar ratio of Au:Pd:Ag = 15:1:1.6 at a reaction temperature of 120 °C. The particles exhibit well-defined facets with an average long edge length of 195 nm. SEM images at high magnifications (Figure 1B, C) revealed that the majority of the particles have a ditetragonal prism (DTP) shape with truncated ends. Particles with this shape are enclosed with 12 faces: eight side faces parallel to the principal axis and two terminating faces located at each of the two ends. A schematic drawing of this shape is presented in Figure 1F, which illustrates the projections of such a particle at

dx.doi.org/10.1021/jp111997s |J. Phys. Chem. C 2011, 115, 3638–3645

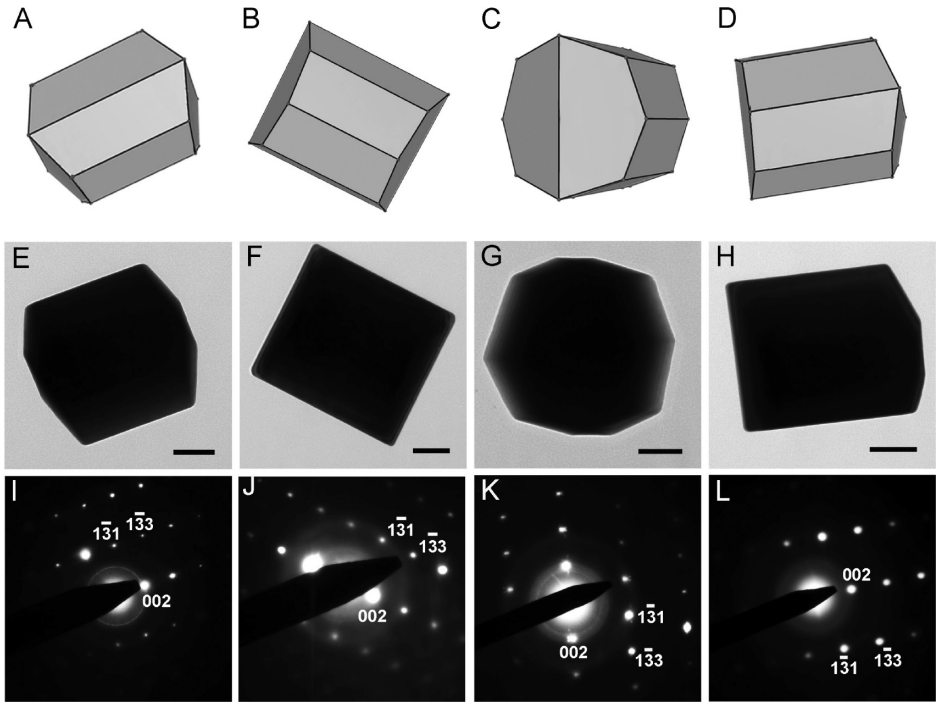

Figure 2. (A−D) The shape models, (E,F) TEM images, and (I−L) corresponding SAED patterns of four Au truncated DTPs with one face parallel to the carbon film of the TEM grids. All SAED patterns show {310} zone axes, indicating that the nanoprisms are enclosed by {310} facets.

different viewing angles. The TEM projection along the principal axis parallel to the prism side faces shows a ditetragonal cross-section (Figure 1D), with measured inner angles alternating between 143° and 127°. These measured angles match well with those calculated from an ideal DTP with high-index {310} side faces, which are 143.1° and 126.9°, respectively (Figure S1).[11,49] This indicates that the side faces of the Au nanocrystals are {310} facets. For a DTP, the principal axis parallel to the eight side faces is [100]. This is confirmed from the HRTEM image of a Au nanoparticle, which shows (200) lattice planes along its principal axis (Figure 1E).

To further confirm the facets of the truncated prisms, we recorded a number of electron diffraction (ED) patterns from particles with either one end face or a side face parallel to the carbon film of the TEM grids. Figure 2 shows four representative ED patterns together with the corresponding TEM images and crystal models. All ED patterns exhibit a [310] zone axis, indicating that both the side and the end faces of the Au nanocrystals are {310} facets. It should be noted that, although a majority of the Au nanocrystals display a shape of truncated DTP as illustrated in Figure 1F, particles with a few slightly different forms were also observed. On the basis of extensive analyses of SEM and TEM images, we carefully established the models of these particles (Figure S2). Similar to the truncated DTPs, these particles are also enclosed with 12 {310} facets.

In addition to truncated DTPs, we also synthesized Au bipyramids in high yield (>90%) following the similar reactions but with higher ratio of Ag(I)/Pd(II) concentrations. Figure 3 shows the morphology of the Au bipyramids obtained at a ratio of Au:Pd:Ag = 15:1:8 with a reaction temperature of 120 °C. FESEM images (Figure 3A,B) indicate that the Au bipyramids have faceted sides and truncated tips. The average base length and height of the bipyramids are 51 and 127 nm, respectively. The truncated tips display a pentagonal shape (Figure 3B, inset). TEM images of the Au bipyramids (Figure 3C,D) show twinned planes, indicating that the Au bipyramids have a 5-fold twinned structure. This 5-fold twinned structure has been previously observed from Au nanorods and bipyramids.[29,31,50−52] Lattice fringes of the bipyramid (Figure 3D) match well with Au (111) planes. The SAED pattern (Figure 3E) of the bipyramids showed the superposition of two sets of patterns characteristic of $[1\bar{1}0]$ and $[1\bar{1}\bar{1}]$ zone diffractions of fcc gold. This result not only confirmed the 5-fold twinned structure of the Au bipyramids but also revealed the ⟨110⟩ growth direction.[51]

In recognition of the effect of Pd(II) and Ag(I) ions on controlling the shape of the Au nanocrystals, we also lowered the Ag/Pd ratio by reducing the concentration of the Ag(I) in the reactions, which led to the formation of truncated tetrahexahedra enclosed by {111} and {310} facets. Figure 4A shows the nanocrystals prepared at a ratio of Au:Pd:Ag = 15:1:0.4. The average diameter of the truncated THHs is about 99 nm. The SEM image at higher magnification (Figure 4B) revealed exposed pentagonal and hexagonal faces, with each hexagonal face surrounded by 6 pentagonal ones. The homogeneous contrast under TEM (Figure 4C) is attributed to the single-crystallinity of the particles. Electron diffraction patterns taken from a number of Au nanocrystals showed both [310] and [111] zone axes (Figure 4D,E), indicating that the exposed faces include both {310} and {111} facets. Careful analyses of the SEM images and diffraction patterns indicated that these nanocrystals are truncated Au THHs. A THH can be seen as a cube with one square pyramid covering each face, forming 24 exposed high-index {*hk*0} ($h \neq k \neq 0$) facets.[11] When a THH bounded by {310} facets is truncated with {111} planes at the eight corners, as illustrated in Figure 4F, a truncated THH with 8 {111} facets in hexagonal shape and 24 {310} facets in pentagonal shape can be formed.

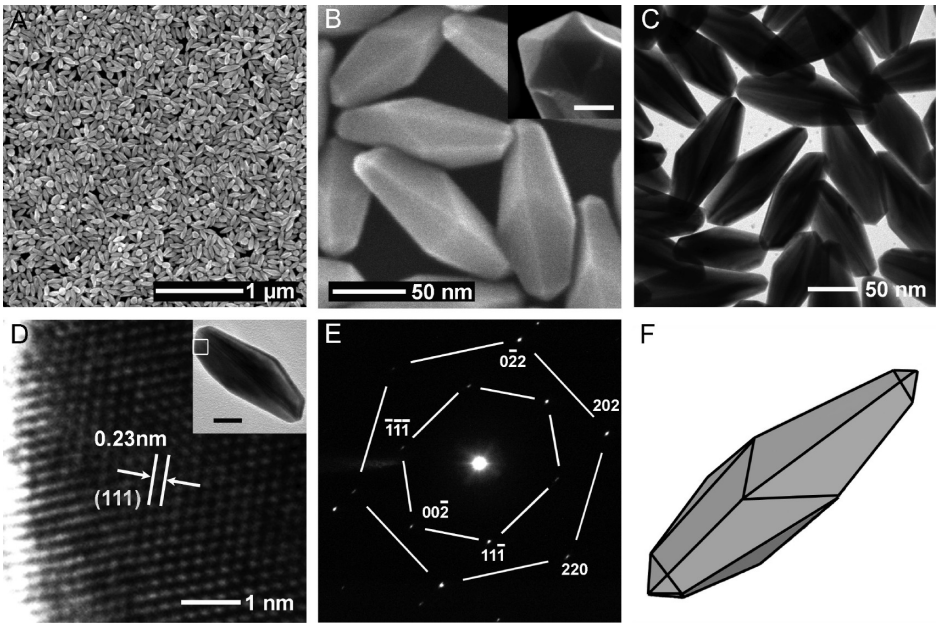

Figure 3. (A) Low- and (B) high-magnification SEM images of Au bipyramids synthesized at a ratio of Au:Pd:Ag = 15:1:8 at a reaction temperature of 120 °C. The truncated tips of the bipyramids with larger sizes show a pentagonal shape (B, inset, scale bar is 100 nm). (C) TEM image of the Au bipyramids clearly shows twin-planes within the nanocrystals. (D) HRTEM image of a bipyramid (inset: the corresponding LRTEM image, scale bar is 20 nm) and (E) its SAED pattern. The SAED pattern shows the superposition of both $[1\bar{1}0]$ and $[1\bar{1}\bar{1}]$ zones of fcc gold. (F) Schematic drawing of a Au bipyramid.

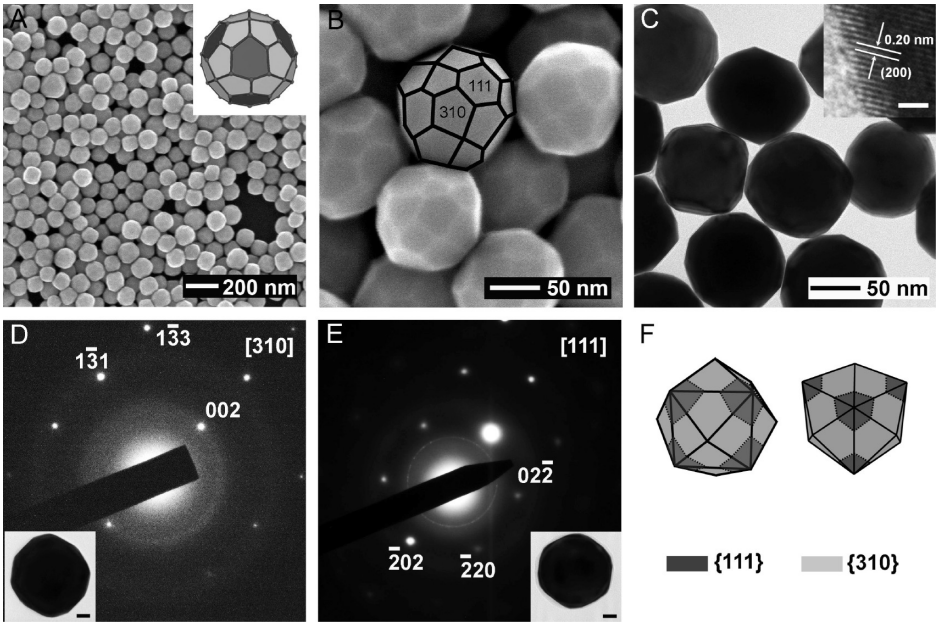

Figure 4. (A) Low- and (B) high-magnification SEM images of Au truncated THHs synthesized at a ratio of Au:Pd:Ag = 15:1:0.4 at 120 °C. (C) TEM image of the truncated THHs with the inset HRTEM showing (200) lattice planes. (D,E) SAED patterns of the Au truncated THHs showing both [310] and [111] zone axes. (F) Schematic illustration, from two different viewing angles, of a THH bounded by {310} facets with {111} planes indicated at 8 corners. The inset of (A) shows a {111} truncated THH.

The composition of the nanocrystals was analyzed using EDX on SEM. It was found that the DTPs are mainly composed of Au (>98 at. %), with a trace amount of Ag (0.4%) and Pd (1.2%) (Figure S3). This is consistent with the ICP-MS measurement, which gave 98.4%, 1%, and 0.6% of Au, Ag, and Pd, respectively. The initial Pd and Ag ions added to the reactions were 6% and 9%, respectively, much higher than the EDX and ICP-MS measurements. This result indicates that Ag and Pd ions were not fully reduced and incorporated into the Au nanocrystals. XPS analysis of the same sample, however, showed higher atomic percentages of Ag and Pd, which accounted for 11% and 19%, respectively (Figure S4). Because the penetration depth of XPS is about 3 nm, the much higher concentrations of Ag and Pd from XPS measurements indicate that they are mainly located at the

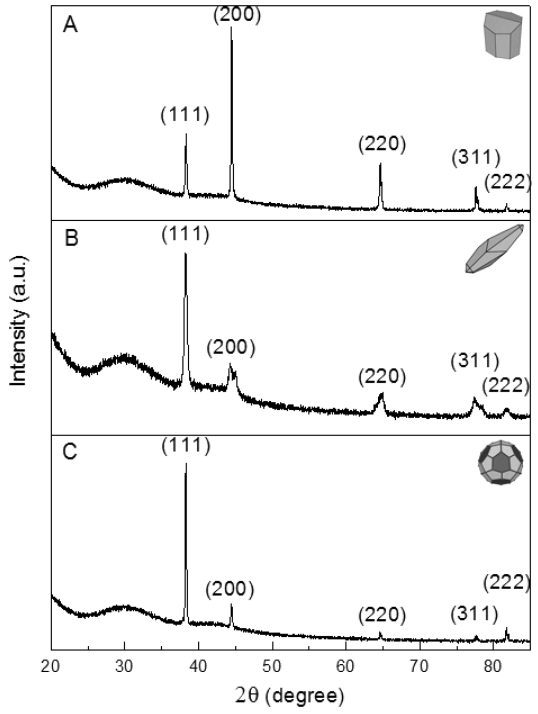

Figure 5. XRD patterns of the Au nanocrystals with different shapes: (A) truncated DTPs, (B) bipyramids, and (C) truncated THHs. The broad peak at 30° is from the substrate.

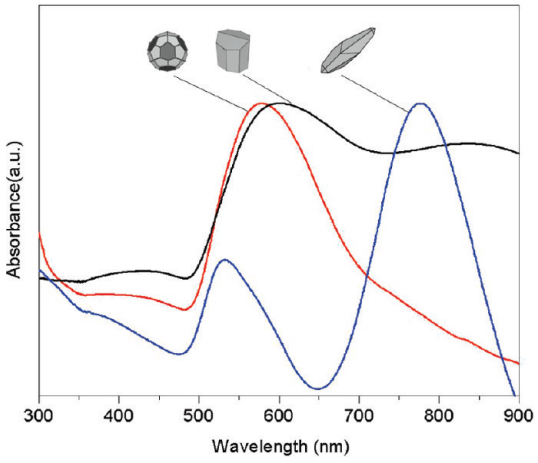

Figure 6. UV−vis spectra of the Au truncated DTPs, bipyramids, and truncated THHs.

surface of the nanocrystals. It is thus believed that the truncated DTPs are essentially Au nanocrystals with a thin surface layer rich of Pd and Ag, although a trace amount of Pd and Ag may also be present in the nanocrystal interior. Similar composition profiles were also obtained from EDX, ICP-MS, and XPS analyses of the bipyramids and truncated THHs (summarized in Table S1). These Au nanocrystals with high-index facets and a Pd/Ag-rich surface layer would be interesting for the study of various catalytic reactions.[53]

Figure 5 shows the XRD patterns of the truncated DTPs, bipyramids, and truncated THHs, respectively. The peak positions of all three patterns match well with those of gold with fcc crystal structure. The DTPs exhibited a much stronger (200) reflection peak than the bipyramids and truncated THH particles

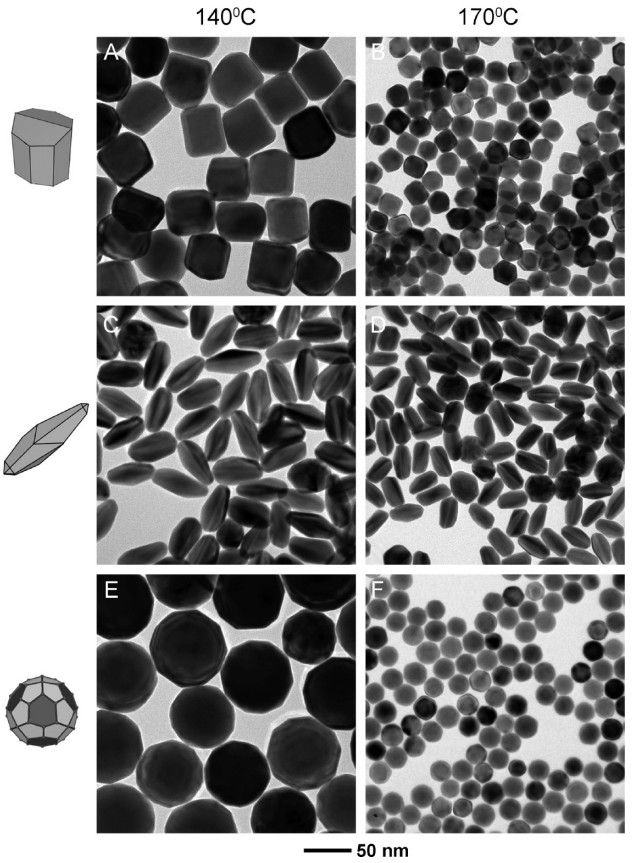

Figure 7. Au nanocrystals synthesized at different temperatures: (A, C, and E) at 140 °C and (B, D, and F) at 170 °C. (A,B) Truncated DTPs with average edge lengths of 52 and 30 nm obtained at a ratio of Au:Pd:Ag = 15:1:1.6, (C,D) bipyramids with heights of 53 and 40 nm obtained at a ratio of Au:Pd:Ag = 15:1:8, and (E,F) truncated THHs with diameters of 75 and 32 nm obtained at a ratio of Au:Pd:Ag = 15:1:0.4, respectively.

(Figure 5A). The intensity ratios of (111) to (200) and (111) to (220) for DTPs are 0.37 and 1.33, respectively, which are much lower than those of standard powder sample of fcc gold (2 and 3.33, respectively).[30] The relatively stronger (200) and (220) reflections than (111) may be attributed to the abundance of {310} facet, which is a stepped surface composed of (100) terrace and (110) step [3(100) × (110)] (Figure S1).[54] The peak splitting for the Au bipyramids (Figure 5B) may be attributed to the polycrystallinity of the nanocrystals, which induces large strain at the grain boundaries.[55] Another possible reason is due to the presence of impurity phases such as Ag or Pd alloyed with Au.

UV−vis spectra of the Au nanocrystals with three different shapes are presented in Figure 6. The DTPs exhibit a strong surface plasmon resonance (SPR) peak at 600 nm and another broader peak at 836 nm, corresponding to the transversal and longitudinal modes, respectively. The Au bipyramids show a sharp, strong peak at 775 nm and a broad peak at 533 nm. The Au truncated THHs only have one SPR peak at 578 nm due to the more symmetric configuration.

By varying the reaction temperature, Au nanocrystals of the three shapes can be synthesized with different sizes. When the temperature was increased from 120 to 140 and 170 °C, we obtained Au DTPs with edge lengths of 52 and 30 nm, bipyramids with heights of 53 and 40 nm, and truncated THHs

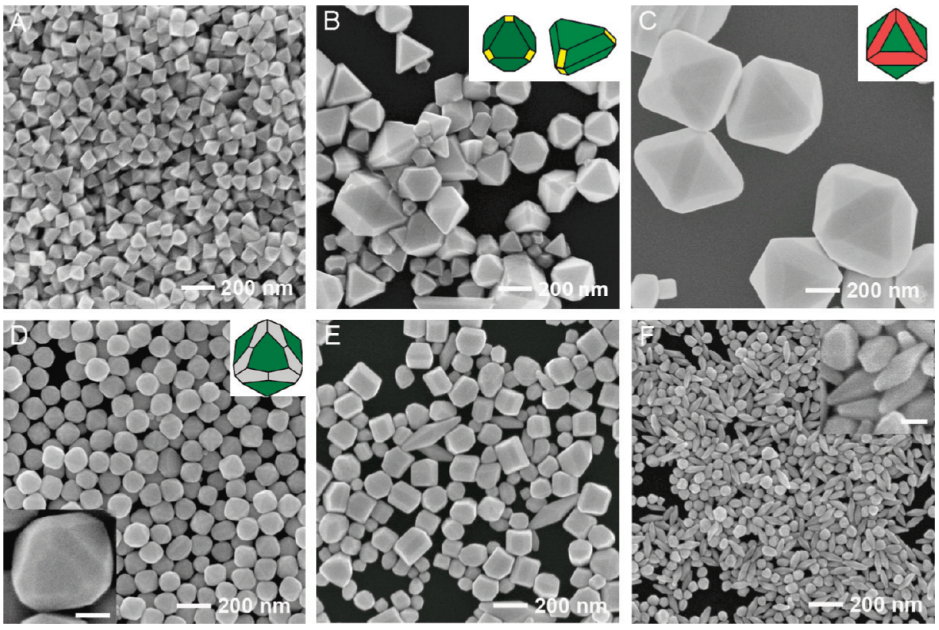

Figure 8. Au nanostructures obtained at different concentrations of Pd and Ag ions: (A) Reaction without adding Pd or Ag ions; (B) Au:Pd = 15:1, but no Ag; (C) Au:Ag = 15:1, but no Pd; (D−F) Au:Pd:Ag = 15:2:0.4, 15:2:1.6, 15:2:8, respectively. Scale bars for insets of (D) and (F) are 50 nm. The reaction temperature for (A) was 195 °C, while for (B−F) it was 120 °C.

with diameters of 75 and 32 nm, respectively (Figure 7). It is clear that at higher temperatures, smaller Au nanostructures were formed. This is because higher reaction temperatures favor the formation of larger number of nuclei at the initial stage and hence smaller extent of nanoparticle growth.

Previously, PDDA-mediated polyol synthesis has been employed to grow Au octahedra.[8] Interestingly, the introduction of Ag and Pd foreign ions in the similar reactions has led to completely different shapes. To further elucidate the effects of Ag and Pd ions on the shape-selective growth of Au nanoparticles, we conducted a series of control experiments by varying the concentrations of Pd(II) and Ag(I) while keeping $AuCl_4^-$ concentration at a constant. Figure 8A shows the Au octahedra enclosed by {111} facets prepared from reactions of $HAuCl_4$ (0.9 mM) and PDDA in EG. When a small amount of Pd(II) (0.06 mM) was added to the reaction, the gold nanocrystals evolved from octahedra to apex truncated octahedra and triangular plates (Figure 8B). These truncations are accompanied by the appearance of {100} facets, which can be attributed to the deposition of Pd. Replacing Pd(II) with Ag(I) showed a different way of truncation. Figures 8C shows Au nanocrystals synthesized in the absence of Pd(II) but with Ag(I) ions at a concentration of 0.06 mM, in which case edge truncated octahedra were formed (Figure 8C). Because the truncated edges of the octahedra are {110} facets, this result indicates that the addition of Ag ions promotes the formation of {110} facets of Au nanocrystals. Reactions with higher concentration of Pd ions (0.12 mM) in the presence of Ag ions were also performed. Figure 8D−F shows the nanocrystals obtained from reactions at ratios of Au:Pd:Ag = 15:2:0.4, 15:2:1.6, and 15:2:8, respectively. Truncated THHs (140 nm), truncated DTPs (250 nm), and bipyramids (130 nm) were formed at these three ratios, but particle sizes are larger than those obtained at low concentration of Pd(II). An SEM image of the truncated THHs at higher magnification showing clearly the different facets is presented in Figure S5. It should be noted that the truncated THHs obtained in this case (Figure 8D) have a higher degree of coverage of {111} facets than those obtained at lower concentration of Pd(II) (Figure 4). In addition, the yields of DTPs and bipyramids are lower than those obtained at a Pd(II) concentration of 0.06 mM. Comparison of the nanocrystals obtained at different Ag(I) and Pd(II) concentrations (Ag/Pd = 0.2:1, Figure 8D; 0.4:1, Figure 4; 0.8:1, Figure 8E; and 1.6:1, Figure 1) shows that the coverage of {310} facets increases with the Ag(I)/Pd(II) ratio until the particles are enclosed entirely by {310} facets. This trend holds at low concentrations of Ag(I) (<0.1 mM). Reactions at higher concentration of Ag(I) lead to the formation of multiple-twinned bipyramids.

Table 1. Summary of the Au Nanocrystals Synthesized in the Presence of Ag(I) and Pd(II) Foreign Ions in a PDDA-Mediated Polyol Process

Foreign ions	Shape of the Au nanocrystals	Facets
Pd(II) only		{111} + {100}
Ag(I) only		{111} + {110}
Low ratio of Ag(I)/Pd(II)		{111} + {310}
High ratio of Ag(I)/Pd(II)		{310}
Very high Ag(I) concentration		

Table 1 summarizes the different shapes of Au nanocrystals formed in the presence of Pd(II) and Ag(I) ions. These results indicate that Ag and Pd promote the formation of different facets; while Ag(I) causes the appearance of {110} facets, Pd(II) facilitates the development of {100} facets. These two foreign ions in combination lead to high-index {310} facets. The role of Ag(I) in controlling the shape of Au nanocrystals has been

dx.doi.org/10.1021/jp111997s |J. Phys. Chem. C 2011, 115, 3638–3645

investigated in various syntheses.[22] Mechanisms such as adsorption of silver halide layer on Au {110} faces[28] or different UPD shifts of Ag on Au surfaces ({110} > {100} > {111})[29] have been suggested. In either case, it is the preferred deposition of Ag species on Au {110} surface that inhibits the growth perpendicular to these facets. It is worth noting that the preferred deposition of Ag on Au crystal facets can also be affected by the anions and capping ligands. It has been found that when different capping ligands were used, Ag UPD may favor the growth of either {110} or {100} facet.[35] Deposition of Pd may also take place on the surface of Au crystals.[39,56,57] It has been found that adsorption energies of Pd on Au {100} and {110} facets are nearly the same but higher than that of {111}.[58] However, other contributions, especially the adsorption of capping ligand (PDDA) and anions, may strongly change the energetics of the system.[59,60] It is possible that in the presence of PDDA and $PdCl_4^{2-}$ ions, Pd deposition preferably takes place on Au {100}. When both Pd(II) and Ag(I) at low concentrations are used, the competition of Ag and Pd deposition on respective Au {110} and {100} facets eventually leads to the appearance of {310} facet, which is a stepped facet containing a 3-atomic wide {100} terrace and one {110} step. For reactions with high concentration of Ag(I), Cl^- dissociated from PDDA can react with $AgNO_3$ to form AgCl precipitate, which may serve as seeds for the growth of Au twinned particles.[61] These multiple-twinned particles eventually develop into bipyramids with high-index facets mediated by the codeposition of Ag and Pd. It is worth noting that, in addition to the difference in selective adsorption of Ag and Pd ions on Au surface, galvanic-assisted reduction[10] may also play a role in the growth of particular facets. During the reaction, Ag and Pd deposited onto the surface of a Au crystal can be oxidized by $AuCl_4^-$. Therefore a continuous deposition and dissolution process takes place on the nanocrystal surface partially occupied by Ag, Pd, and Au. Because of the lattice mismatch among Ag, Pd, and Au (with lattice constants of 0.409, 0.389, and 0.408 nm, respectively), the growth mode of Au on such a crystal surface will be different from that on pure gold, leading to the formation of high-index facets.

CONCLUSIONS

We have presented a new route to Au nanoparticles with high-index facets by using a facile one-pot PDDA-mediated polyol process with the assistance of Ag(I) and Pd(II) foreign ions. Various shapes including Au truncated DTPs enclosed by 12 {310} facets, truncated THHs with both {111} and {310} facets, and multiple-twinned bipyramids facets were obtained in high yields (>90%) and in a wide range of sizes (50−250 nm). It was found that when introduced separately, Ag(I) and Pd(II) ions cause {110} and {100} truncations of Au octahedra, respectively. The presence of both Ag(I) and Pd(II) is critical for the growth of high-index facets. At low concentrations of Ag(I), simultaneous deposition of Ag and Pd on Au crystal surface serves to inhibit the growth along ⟨310⟩ direction that leads to the formation of Au truncated THHs partially enclosed by {310} facets and truncated DTPs entirely bounded by {310} facets. When the Ag(I) concentration is relatively high (>1/2 of $AuCl_4^-$ concentration), multiple-twinned bipyramids were formed. Elemental analyses indicate that these nanocrystals are mainly composed of Au with a surface layer rich in Ag and Pd.

ASSOCIATED CONTENT

Supporting Information. Further details on shape models, elemental analyses, and more SEM images. This material is available free of charge via the Internet at http://pubs.acs.org.

AUTHOR INFORMATION

Corresponding Author
*E-mail: chelxm@nus.edu.sg.

ACKNOWLEDGMENT

We are thankful for financial support from the Ministry of Education Singapore, under research projects R-279-000-273-133/298-112.

REFERENCES

(1) Xia, Y.; Xiong, Y.; Lim, B.; Skrabalak, S. E. *Angew. Chem., Int. Ed.* **2009**, *48*, 60–103.
(2) Sau, T. K.; Rogach, A. L. *Adv. Mater.* **2010**, *22*, 1781–1804.
(3) Glotzer, S. C.; Solomon, M. J. *Nat. Mater.* **2007**, *6*, 557–562.
(4) Habas, S. E.; Lee, H.; Radmilovic, V.; Somorjai, G. A.; Yang, P. *Nat. Mater.* **2007**, *6*, 692–697.
(5) Huang, X.; Neretina, S.; El-Sayed, M. A. *Adv. Mater.* **2009**, *21*, 4880–4910.
(6) Huang, X.; Tang, S.; Zhang, H.; Zhou, Z.; Zheng, N. *J. Am. Chem. Soc.* **2009**, *131*, 13916–13917.
(7) Niu, W.; Zheng, S.; Wang, D.; Liu, X.; Li, H.; Han, S.; Chen, J.; Tang, Z.; Xu, G. *J. Am. Chem. Soc.* **2009**, *131*, 697–703.
(8) Li, C.; Shuford, K. L.; Chen, M.; Lee, E. J.; Cho, S. O. *ACS Nano* **2008**, *2*, 1760–1769.
(9) Niu, W.; Zhang, L.; Xu, G. *ACS Nano* **2010**, *4*, 1987–1996.
(10) Zhou, Z.-Y.; Tian, N.; Huang, Z.-Z.; Chen, D.-J.; Sun, S.-G. *Faraday Discuss.* **2009**, *140*, 81–92.
(11) Tian, N.; Zhou, Z.-Y.; Sun, S.-G.; Ding, Y.; Wang, Z. L. *Science* **2007**, *316*, 732–735.
(12) Tian, N.; Zhou, Z.-Y.; Sun, S.-G. *Chem. Commun.* **2009**, 1502–1504.
(13) Ma, Y.; Kuang, Q.; Jiang, Z.; Xie, Z.; Huang, R.; Zheng, L. *Angew. Chem., Int. Ed.* **2008**, *47*, 8901–8904.
(14) Jeong, G. H.; Kim, M.; Lee, Y. W.; Choi, W.; Oh, W. T.; Park, Q. H.; Han, S. W. *J. Am. Chem. Soc.* **2009**, *131*, 1672–1673.
(15) Wu, H. L.; Kuo, C. H.; Huang, M. H. *Langmuir* **2010**, *26*, 12307–12313.
(16) Tao, A. R.; Habas, S.; Yang, P. D. *Small* **2008**, *4*, 310–325.
(17) Chang, C.-C.; Wu, H.-L.; Kuo, C.-H.; Huang, M. H. *Chem. Mater.* **2008**, *20*, 7570–7574.
(18) Sau, T. K.; Murphy, C. J. *J. Am. Chem. Soc.* **2004**, *126*, 8648–8649.
(19) Seo, D.; Yoo, C. I.; Chung, I. S.; Park, S. M.; Ryu, S.; Song, H. *J. Phys. Chem. C* **2008**, *112*, 2469–2475.
(20) Yu, Y.; Zhang, Q.; Lu, X.; Lee, J. Y. *J. Phys. Chem. C* **2010**, *114*, 11119–11126.
(21) Chen, Y. H.; Hung, H. H.; Huang, M. H. *J. Am. Chem. Soc.* **2009**, *131*, 9114–9121.
(22) Grzelczak, M.; Pérez-Juste, J.; Mulvaney, P.; Liz-Marzán, L. M. *Chem. Soc. Rev.* **2008**, *37*, 1783–1791.
(23) Krichevski, O.; Markovich, G. *Langmuir* **2007**, *23*, 1496–1499.
(24) Lu, D.-L.; Ichihara, M.; Tanaka, K.-I. *Electrochim. Acta* **1998**, *43*, 2325–2330.
(25) Lu, D.-l.; Tanaka, K.-I. *J. Electroanal. Chem.* **1997**, *430*, 69–76.
(26) Song, H.; Kim, F.; Connor, S.; Somorjai, G. A.; Yang, P. *J. Phys. Chem. B* **2005**, *109*, 188–193.
(27) Sun, J.; Guan, M.; Shang, T.; Gao, C.; Xu, Z.; Zhu, J. *Cryst. Growth Des.* **2008**, *8*, 906–910.

(28) Jana, N. R.; Gearheart, L.; Murphy, C. J. *Adv. Mater.* **2001**, *13*, 1389–1393.
(29) Liu, M.; Guyot-Sionnest, P. *J. Phys. Chem. B* **2005**, *109*, 22192–22200.
(30) Seo, D.; Park, J. C.; Song, H. *J. Am. Chem. Soc.* **2006**, *128*, 14863–14870.
(31) Kou, X.; Ni, W.; Tsung, C.-K.; Chan, K.; Lin, H.-Q.; Stucky, G. D.; Wang, J. *Small* **2007**, *3*, 2103–2113.
(32) Seo, D.; Yoo, C. I.; Park, J. C.; Park, S. M.; Ryu, S.; Song, H. *Angew. Chem., Int. Ed.* **2008**, *47*, 763–767.
(33) Xiang, Y.; Wu, X.; Liu, D.; Feng, L.; Zhang, K.; Chu, W.; Zhou, W.; Xie, S. *J. Phys. Chem. C* **2008**, *112*, 3203–3208.
(34) Ming, T.; Feng, W.; Tang, Q.; Wang, F.; Sun, L.; Wang, J.; Yan, C. *J. Am. Chem. Soc.* **2009**, *131*, 16350–16351.
(35) Hsu, S. J.; Su, P. Y. S.; Jian, L. Y.; Chang, A. H. H.; Lin, I. J. B. *Inorg. Chem.* **2010**, *49*, 4149–4155.
(36) Kim, F.; Song, J. H.; Yang, P. *J. Am. Chem. Soc.* **2002**, *124*, 14316–14317.
(37) Kim, F.; Connor, S.; Song, H.; Kuykendall, T.; Yang, P. *Angew. Chem., Int. Ed.* **2004**, *43*, 3673–3677.
(38) Zhang, J.; Langille, M. R.; Personick, M. L.; Zhang, K.; Li, S.; Mirkin, C. A. *J. Am. Chem. Soc.* **2010**, *132*, 14012–14014.
(39) Fan, F.-R.; Liu, D.-Y.; Wu, Y.-F.; Duan, S.; Xie, Z.-X.; Jiang, Z.-Y.; Tian, Z.-Q. *J. Am. Chem. Soc.* **2008**, *130*, 6949–6951.
(40) Grzelczak, M.; Pérez-Juste, J.; Rodrıguez-González, B.; Liz-Marzán, L. M. *J. Mater. Chem.* **2006**, *16*, 3946–3946.
(41) Xiang, Y.; Wu, X.; Liu, D.; Jiang, X.; Chu, W.; Li, Z.; Ma, Y.; Zhou, W.; Xie, S. *Nano Lett.* **2006**, *6*, 2290–2294.
(42) Song, J. H.; Kim, F.; Kim, D.; Yang, P. D. *Chem.-Eur. J.* **2005**, *11*, 910–916.
(43) Ferrer, D.; Torres-Castro, A.; Gao, X.; Sepúlveda-Guzmán, S.; Ortiz-Méndez, U.; José-Yacamán, M. *Nano Lett.* **2007**, *7*, 1701–1705.
(44) Lee, Y. W.; Kim, M.; Kim, Z. H.; Han, S. W. *J. Am. Chem. Soc.* **2009**, *131*, 17036–17037.
(45) Lim, B.; Kobayashi, H.; Yu, T.; Wang, J.; Kim, M. J.; Li, Z.-Y.; Rycenga, M.; Xia, Y. *J. Am. Chem. Soc.* **2010**, *132*, 2506–2507.
(46) Lu, C.-L.; Prasad, K. S.; Wu, H.-L.; Ho, J.-A. A.; Huang, M. H. *J. Am. Chem. Soc.* **2010**, *132*, 14546–14553.
(47) Ding, Y.; Fan, F.; Tian, Z.; Wang, Z. L. *J. Am. Chem. Soc.* **2010**, *132*, 12480–12486.
(48) Ferrando, R.; Jellinek, J.; Johnston, R. L. *Chem. Rev.* **2008**, *108*, 845–910.
(49) Tian, N.; Zhou, Z. Y.; Sun, S. G. *J. Phys. Chem. C* **2008**, *112*, 19801–19817.
(50) Johnson, C. J.; Dujardin, E.; Davis, S. A.; Murphy, C. J.; Mann, S. *J. Mater. Chem.* **2002**, *12*, 1765–1770.
(51) Kou, X.; Zhang, S.; Tsung, C.-K.; Yeung, M. H.; Shi, Q. Stucky, G. D.; Sun, L.; Wang, J.; Yan, C. *J. Phys. Chem. B* **2006**, *110*, 16377–16383.
(52) Wu, H.-L.; Chen, C.-H.; Huang, M. H. *Chem. Mater.* **2009**, *21*, 110–114.
(53) Chen, M.; Kumar, D.; Yi, C.-W.; Goodman, D. W. *Science* **2005**, *310*, 291–293.
(54) Van Hove, M. A.; Somorjai, G. A. *Surf. Sci.* **1980**, *92*, 489–518.
(55) Li, C. C.; Sato, R.; Kanehara, M.; Zeng, H. B.; Bando, Y.; Teranishi, T. *Angew. Chem., Int. Ed.* **2009**, *48*, 6883.
(56) Kibler, L.; Kleinert, M.; Randler, R.; Kolb, D. M. *Surf. Sci.* **1999**, *443*, 19–30.
(57) Stafford, G. R.; Bertocci, U. *J. Phys. Chem. C* **2009**, *113*, 261–268.
(58) Kibler, L.; Kleinert, M.; Lazarescu, V.; Kolb, D. M. *Surf. Sci.* **2002**, *498*, 175–185.
(59) Naohara, H.; Ye, S.; Uosaki, K. *J. Phys. Chem. B* **1998**, *102*, 4366–4373.
(60) Rojas, M. I.; G., M.; Leiva, E. P. M. *Langmuir* **2000**, *16*, 9539–9546.
(61) Im, S. H.; Lee, Y. T.; Wiley, B.; Xia, Y. *Angew. Chem., Int. Ed.* **2005**, *44*, 2154–2157.